Spectrochimica Acta Part A: Molecular and Biomolecular Spectroscopy 104 (2013) 1–13

Contents lists available at SciVerse ScienceDirect

Spectrochimica Acta Part A: Molecular and Biomolecular Spectroscopy

journal homepage: www.elsevier.com/locate/saa

Structural, thermal, morphological and biological studies of proton-transfer complexes formed from 4-aminoantipyrine with quinol and picric acid

Abdel Majid A. Adam *

Department of Chemistry, Faculty of Science, Taif University, Al-Haweiah, P.O. Box 888, Zip Code 21974, Taif, Saudi Arabia

HIGHLIGHTS

- Two new CT complexes of 4-aminoantipyrine with QL and PA are obtained.
- Various spectroscopic and thermal analysis are used.
- The complex obtained with PA has a remarkable morphology and good thermal stability.

GRAPHICAL ABSTRACT

Sponge-like morphology of [(4AAP)(PA)] complex.

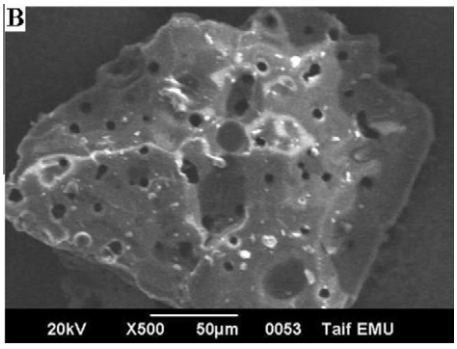

ARTICLE INFO

Article history:
Received 13 October 2012
Received in revised form 12 November 2012
Accepted 15 November 2012
Available online 29 November 2012

Keywords:
4-Aminoantipyrine
Proton-transfer
XRD
SEM
Thermal analysis

ABSTRACT

4-Aminoantipyrine (4AAP) is widely used in the pharmaceutical industry, biochemical experiments and environmental monitoring. However, residual amounts of 4AAP in the environment may pose a threat to human health. To provide basic data that can be used to extract or eliminate 4AAP from the environment, the proton-transfer complexes of 4AAP with quinol (QL) and picric acid (PA) were synthesized and spectroscopically investigated. The interactions afforded two new proton-transfer salts named 1,5-dimethyl-3-oxo-2-phenyl-2,3-dihydro-1*H*-pyrazol-4-aminium-4-hydroxyphenolate and 1,5-dimethyl-3-oxo-2-phenyl-2,3-dihydro-1*H*-pyrazol-4-aminium-2,4,6-trinitrophenolate for QL and PA, respectively, via a 1:1 stoichiometry. Elemental analysis (CHN), electronic absorption, spectrophotometric titration, IR, Raman, ^{1}H NMR and X-ray diffraction were used to characterize the new products. The thermal stability of the synthesized CT complexes was investigated using thermogravimetric (TG) analyses, and the morphology and particle size of these complexes were obtained from scanning electron microscopy (SEM). It was found that PA and 4AAP immediately formed a yellow precipitate with a remarkable sponge-like morphology and good thermal stability up to 180 °C. Finally, the biological activities of the newly synthesized CT complexes were tested for their antibacterial and antifungal activities. The results indicated that the [(4AAP)(QL)] complex exhibited strong antimicrobial activities against various bacterial and fungal strains compared with standard drugs.

* Tel.: +966 2727 2020/502099808; fax: +966 2727 4299.
E-mail address: majidadam@yahoo.com

1386-1425/$ - see front matter © 2012 Elsevier B.V. All rights reserved.
http://dx.doi.org/10.1016/j.saa.2012.11.042

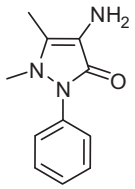

Formula I. Molecular structure of 4-aminoantipyrine.

Introduction

4-Aminoantipyrine (4AAP, Formula I) is a metabolite of aminophenazone and is an aromatic substance with analgesic, antipyretic, antiphlogistic and anti-inflammatory properties [1–6]. Although today 4AAP is scarcely ever administered as an analgesic drug because of its side effects, it is still used as a precursor of 4AAP derivatives, which have better biological activities [7,8]. In addition, the compound is used as a reagent for biochemical reactions that produce peroxides or phenols [9,10] and can also be used to detect phenols in the environment [11]. Because 4AAP is widely used in pharmacological [12], clinical [13], biological, biochemical [14] and analytical applications [15], as well as in environmental monitoring, 4AAP has become an environmental pollutant [16]. The toxic effect of 4AAP on animals has been reported experimentally [17]. 4AAP can reduce blood flow [18] and form stable complexes with heme [19]; moreover, it has an obvious denaturing effect on bovine hemoglobin [20]. In recent years, 4AAP transition metal complexes and their derivatives have been extensively examined due to their wide biological, analytical and therapeutic applications. Furthermore, they have been investigated due to their diverse biological properties as antifungal, antibacterial, analgesic, sedative, antipyretic, anti-inflammatory and DNA-binding agents [21–24].

This paper aims to investigate the 4AAP charge-transfer complexes, which are readily prepared from the reaction of 4AAP with quinol (benzene-1,4-diol, QL) and picric acid (2,4,6-trinitrophenol, PA). The synthesized CT complexes were structurally characterized using elemental analysis; infrared (IR), Raman, ^{1}H NMR and electronic absorption spectroscopy; powder X-ray diffraction; and scanning electron microscopy (SEM). The thermal behavior of the obtained complexes and the kinetic and thermodynamic parameters (E^*, A, ΔS^*, ΔH^* and ΔG^*) were also investigated. Finally, the antimicrobial activity of the 4AAP complexes was determined against various bacterial and fungal strains.

Experimental

Reagents

4-Aminoantipyrine (4AAP) ($C_{11}H_{13}N_3O$) was obtained from Sigma–Aldrich Chemical Company, USA, with a stated purity of greater than 99% and was used without further purification. Quinol (benzene-1,4-diol, QL) and picric acid (2,4,6-trinitrophenol, PA) were purchased from Merck Chemical Co. and were also used as received.

Synthetic procedure

The solid CT complexes of 4AAP with QL or PA were synthesized by mixing 1 mmol 4AAP with 1 mmol of each acceptor in methanol (10 ml). The mixtures were stirred at room temperature for 10 min, which resulted in the precipitation of the products. In the 4AAP/QL system, upon addition of QL to a solution of 4AAP, the color of the solution changed from light yellow to red to reddish-brown. A dark reddish-brown precipitate was filtered off, washed several times with methanol and then dried under vacuum over anhydrous calcium chloride. In the case of the 4AAP/PA complex, upon addition of PA to 4AAP dissolved in methanol, a yellow precipitate formed immediately.

Spectrophotometric titration measurements

Spectrophotometric titration measurements were performed for the reactions of 4AAP with QL or PA against methanol as a blank at wavelengths of 286 and 281 nm, respectively. A 0.25, 0.50, 0.75, 1.00, 1.50, 2.0, 2.50, 3.00, 3.50 or 4.00 ml aliquot of a standard solution (5.0×10^{-4} M) of the appropriate acceptor in MeOH was added to 1.00 ml of 5.0×10^{-4} M 4AAP, which was also dissolved in MeOH. The total volume of the mixture was 5 ml. The concentration of 4AAP (C_d) in the reaction mixture was maintained at 5.0×10^{-4} M, whereas the concentration of the acceptors (C_a) changed over a wide range of concentrations (0.25×10^{-4} M to 4.00×10^{-4} M) to produce solutions with an acceptor molar ratio that varied from 4:1 to 1:4. The stoichiometry of the molecular CT complexes was obtained from the determination of the conventional spectrophotometric molar ratio according to known methods [25] using a plot of the absorbance of each CT complex as a function of the C_d:C_a ratio. Modified Benesi–Hildebrand plots were constructed [26,27] to allow the calculation of the formation constant, K_{CT}, and the absorptivity, ε_{CT}, values for each CT complex in this study.

Instrumental analyses

Elemental analyses

The elemental analyses of the carbon, hydrogen and nitrogen contents were performed by the microanalysis facility at Cairo University, Egypt, using a Perkin–Elmer CHN 2400 (USA).

Electronic spectra

The electronic absorption spectra of methanolic solutions of the donor, acceptors and resulting CT complexes were recorded over a wavelength range of 200–800 nm using a Perkin–Elmer Lambda 25 UV/Vis double-beam spectrophotometer at Taif University, Saudi Arabia. The instrument was equipped with a quartz cell with a 1.0 cm path length.

Infrared and Raman spectra

The mid-infrared (IR) spectra (KBr discs) within the range of 4000–400 cm^{-1} for the solid CT complexes were recorded on a Shimadzu FT-IR spectrophotometer with 30 scans at 2 cm^{-1} resolution. The Raman laser spectra of the samples were measured on a Bruker FT-Raman spectrophotometer equipped with a 50 mW laser at Taif University, Saudi Arabia.

^{1}H NMR spectra

^{1}H NMR spectra were collected by the Analytical Center at King Abdul Aziz University, Saudi Arabia, on a Bruker DRX-250 spectrometer operating at 250.13 MHz with a dual 5 mm probe head. The measurements were performed at ambient temperature using DMSO-d_6 (dimethylsulfoxide, d_6) as a solvent and TMS (tetramethylsilane) as an internal reference. The ^{1}H NMR data are expressed in parts per million (ppm) and are internally referenced to the residual proton impurity in the DMSO solvent.

Thermal analysis

Thermogravimetric analysis (TGA) was performed under an air atmosphere between room temperature and 800 °C at a heating rate of 10 °C/min using a Shimadzu TGA-50H thermal analyzer at the Central Lab at Ain Shams University, Egypt.

X-ray diffraction patterns

The X-ray diffraction patterns for the obtained CT complexes were collected on a PANalytical X'Pert PRO X-ray powder diffractometer at the Central Lab at Ain Shams University, Egypt. The instrument was equipped with a Ge(III) monochromator, and a Cu $K\alpha_1$ X-ray source with a wavelength of 0.154056 nm was used.

SEM and EDX detection

Scanning electron microscopy (SEM) images and energy-dispersive X-ray spectroscopy (EDX) patterns were collected on a Jeol JSM-6390 instrument at Taif University, Saudi Arabia. The instrument was operated at an accelerating voltage of 20 kV.

Biological assessment

Antibacterial activity

The antimicrobial activities of the newly synthesized 4AAP CT complexes and the pure solvent were tested in vitro against two Gram-positive bacteria, *Staphylococcus aureus* (MSSA 22) and *Bacillus subtilis* (ATCC 6051), and two Gram-negative bacteria, *Escherichia coli* (K 12) and *Pseudomonas aeruginosa* (MTCC 2488), using a modified Bauer–Kirby disc diffusion method [28]. The microanalysis facility at Cairo University, Egypt performed the investigations. For these investigations, 100 μl test bacteria were grown in 10 ml fresh medium until they reached a count of approximately 10^8 - cells/ml for bacteria or 10^5 cells/ml for fungi [29]. Then, 100 μl microbial suspension was spread onto agar plates. The nutrient agar medium for the antibacterial tests consisted of 0.5% peptone, 0.1% beef extract, 0.2% yeast extract, 0.5% NaCl and 1.5% agar-agar [30]. Isolated colonies of each strain were selected from the primary agar plates and tested for susceptibility. After the plates were incubated for 48 h at 37 °C, the inhibition (sterile) zone diameters (including the disc) were measured using slipping calipers from the National Committee for Clinical Laboratory Standards (NCCLS, 1993) [31] and are expressed in mm. The screening was performed using 100 μg/ml CT complex. An antibiotic disc of tetracycline (30 μg/disc, Hi-Media) was used as a positive control.

Antifungal activity

The newly synthesized complexes were also screened for their antifungal properties against *Aspergillus flavus* (laboratory isolate) and *Candida albicans* (IQA-109) in DMSO using a modified Bauer–Kirby disc diffusion method [28]. The complex was dissolved in DMSO. The medium for the antifungal tests consisted of 3% sucrose, 0.3% $NaNO_3$, 0.1% K_2HPO_4, 0.05% KCl, 0.001% $FeSO_4$ and 2% agar-agar [30]. The disc diffusion method for the filamentous fungi was tested using the M38-A standard method [32], whereas the disc diffusion method for yeast was tested using the M44-P standard method [33]. Plates inoculated with filamentous fungi or yeast were incubated for 48 h at 25 °C or 30 °C, respectively. The antifungal activity of the CT complexes was compared with that of amphotericin B (30 μg/disc, Hi-Media) as a standard antifungal agent. Antifungal activity was determined by measuring the diameters of the sterile zone (mm) in triplicate.

Results and discussion

Elemental analysis

Elemental analyses (C, H, and N) of the 4AAP CT complexes were performed, and the obtained results are as follows:

(1) [(4AAP)(QL)]: $C_{17}H_{19}N_3O_3$; Mol. wt. = 313.35; Calc.: %C, 65.10; %H, 6.06; %N, 13.40, Found: %C, 65.37; %H, 5.95; %N, 13.58

(2) [(4AAP)(PA)]; $C_{17}H_{16}N_6O_8$; Mol. wt. = 432.34; Calc.: %C, 47.19; %H, 3.70; %N, 19.43, Found: %C, 46.88; %H, 3.51; %N, 19.70

The resulting values are in good agreement with the calculated values, and the suggested values are in agreement with the molar ratios determined from the spectrophotometric titration curves.

Determination of stoichiometry of the resulting CT complexes

The electronic absorption spectra of the donor 4AAP, acceptors QL and PA and the complexes are shown in Fig. 1. These spectra revealed new absorption bands that are attributed to the CT interactions. These bands are observed at 286 and (281 and 353) nm for the 4AAP/QL and 4AAP/PA complexes, respectively. These peak absorbance values were measured and plotted as a function of the C_d:C_a ratio according to a known method. Spectrophotometric titration plots based on these measurements (Fig. 2) confirmed the complex formation at a ratio (4AAP:acceptor) of 1:1 in both cases. Based on the obtained data, the formed charge-transfer or proton-transfer complexes were formulated as [(4AAP)(QL)] and [(4AAP)(PA)].

Determination of the formation constant and the molar extinction coefficient

The spectrophotometric titrations of the intermolecular charge-transfer complexes formed from the reaction of 4AAP with QL or PA indicated the formation of 1:1 CT complexes; therefore, the formation constant (K_{CT}) and the molar absorptivity (ε) of these

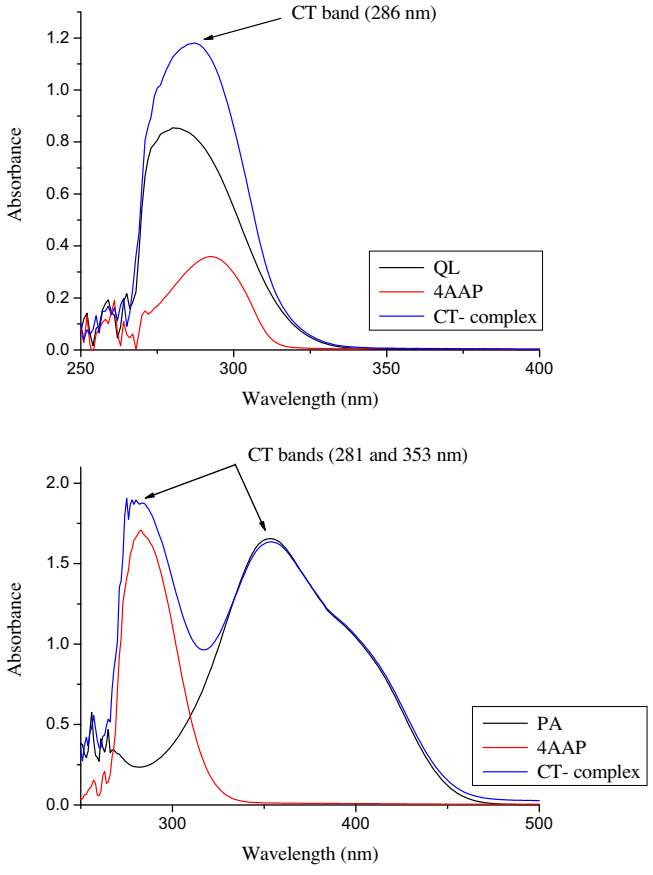

Fig. 1. Electronic absorption spectra of 4AAP-QL and 4AAP-PA CT complexes at the detectable peaks of 286 and (281 and 353) nm, respectively.

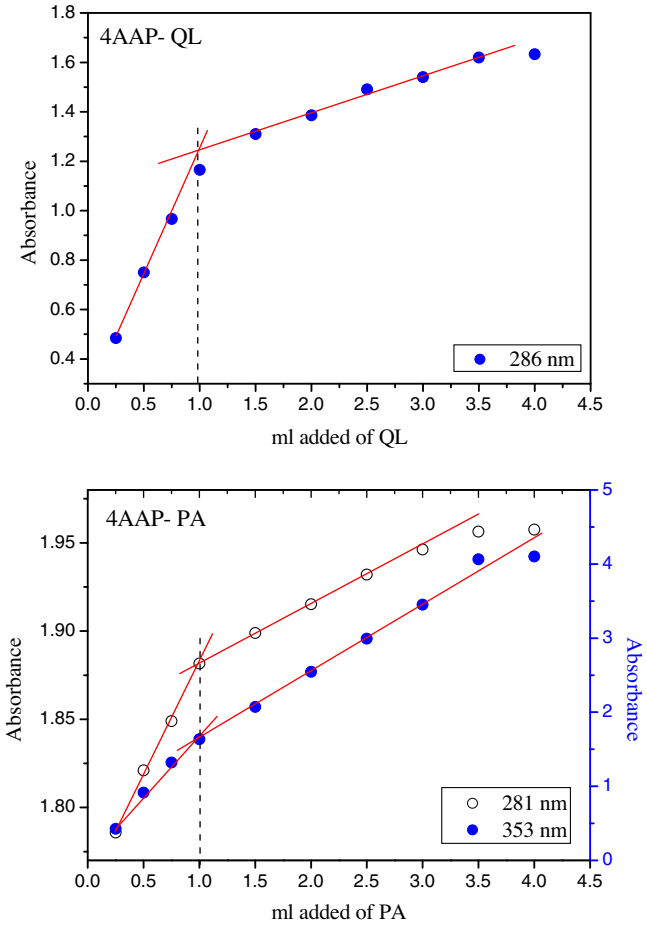

Fig. 2. Spectrophotometric titration curves for 4AAP-QL and 4AAP-PA systems at detectable peaks.

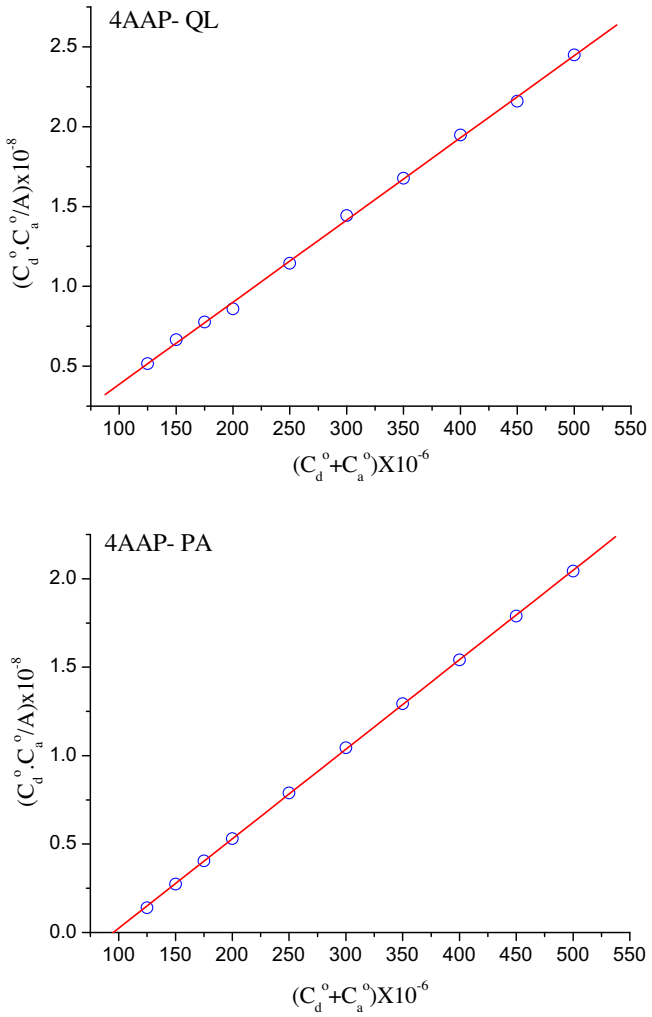

Fig. 3. The modified Benesi–Hildebrand plots of 4AAP-QL and 4AAP-PA systems at detectable peaks of 286 and 281 nm, respectively.

complexes were calculated by applying the 1:1 modified Benesi–Hildebrand equation in the following equation [26]:

$$(C_aC_d)/A = 1/K\varepsilon + (C_a + C_d)/\varepsilon \quad (1)$$

where C_a and C_d are the initial concentrations of the acceptor and the donor, respectively, and A is the absorbance of the strongly detected CT band. When the $(C_aC_d)/A$ values for the 1:1 charge-transfer complex are plotted against the corresponding $(C_a + C_d)$ values, a straight line is obtained with a slope of $1/\varepsilon$ and an intercept of $1/K\varepsilon$. The modified Benesi–Hildebrand plots are shown in Fig. 3, and the values of C_d, C_a, $(C_d + C_a)$ and $(C_dC_a)/A$ are listed in Table 1. The values of both K_{CT} and ε associated with the complexes are given in Table 2. These complexes exhibit high values for both the formation constants (K_{CT}) and the extinction coefficients (ε). The high values of K_{CT} reflect the high stabilities of the formed CT complexes as a result of the expected strong donation from 4AAP, which contains one amine group and nitrogen atoms. The data also reveal that the [(4AAP)(QL)] complex shows a higher K_{CT} value compared with the [(4AAP)(PA)] complex.

Determination of the spectroscopic and physical data

The spectroscopic and physical data, such as the standard free energy (ΔG^o), the oscillator strength (f), the transition dipole moment (μ), the resonance energy (R_N), and the ionization potential (I_P), were estimated for samples dissolved in methanol at 25 °C. The calculations can be summarized as follows.

Determination of oscillator strength (f)

From the CT absorption spectra, the oscillator strength (f) can be estimated using the approximate formula [34]:

$$f = 4.319 \times 10^{-9} \int \varepsilon_{CT} dv \quad (2)$$

where $\int \varepsilon_{CT} dv$ is the area under the curve of the extinction coefficient of the absorption band in question plotted as a function of frequency. To a first approximation:

$$f = 4.319 \times 10^{-9} \varepsilon_{CT} v_{1/2} \quad (3)$$

where ε_{CT} is the maximum extinction coefficient of the CT band, and $v_{1/2}$ is the half-bandwidth in cm^{-1} (i.e., the bandwidth at half of the maximum extinction coefficient value).

Determination of transition dipole moment (μ)

The transition dipole moments (μ) of the complexes have been calculated from the following equation [35]:

$$\mu = 0.0958[\varepsilon_{CT} v_{1/2} / v_{max}]^{1/2} \quad (4)$$

The transition dipole moment can be used to determine if a particular transition is allowed; the transition from a bonding π orbital to an antibonding π^* orbital is allowed because the integral that defines the transition dipole moment is nonzero.

Table 1
The values of C_d, C_a, $C_d + C_a$ and C_dC_a/A, for the 4AAP CT complexes.

Ratio (A:D)	C_d ($\times10^{-4}$)	C_a ($\times10^{-4}$)	$C_d + C_a$ ($\times10^{-6}$)	C_dC_a ($\times10^{-8}$)	4AAP-QL complex		4AAP-PA complex			
					Abs. 286 nm	C_dC_a /A ($\times10^{-8}$)	Abs. 281 nm	C_dC_a /A ($\times10^{-8}$)	Abs. 353 nm	C_dC_a /A ($\times10^{-8}$)
0.25	1.00	0.25	125	0.25	0.4844	0.5161	1.7858	0.1400	0.4259	0.1400
0.50	1.00	0.50	150	0.50	0.7507	0.6660	1.8211	0.2746	0.9149	0.2746
0.75	1.00	0.75	175	0.75	0.9664	0.7761	1.8490	0.4056	1.3214	0.4056
1.00	1.00	1.00	200	1.00	1.1648	0.8585	1.8816	0.5315	1.6356	0.5315
1.50	1.00	1.50	250	1.50	1.3101	1.1450	1.8989	0.7899	2.0712	0.7899
2.00	1.00	2.00	300	2.00	1.3859	1.4431	1.9152	1.0443	2.5453	1.0443
2.50	1.00	2.50	350	2.50	1.4909	1.6768	1.9321	1.2939	2.9929	1.2939
3.00	1.00	3.00	400	3.00	1.5404	1.9475	1.9462	1.5415	3.4511	1.5415
3.50	1.00	3.50	450	3.50	1.6201	2.1604	1.9564	1.7890	4.0631	1.7890
4.00	1.00	4.00	500	4.00	1.6327	2.4499	1.9575	2.0434	4.1010	2.0434

Table 2
Spectrophotometric results of the 4AAP CT complexes.

Complex	λ_{max} (nm)	E_{CT} (eV)	K (Lmol^{-1})	ε_{max} (Lmol^{-1}cm^{-1})	f	μ	I_p	D	R_N	ΔG^o (25 °C) (kJmol^{-1})
[(4AAP)(QL)]	286	4.349	4.02×10^4	1.95×10^4	21.01	35.73	11.11	32.70	1.23	−37,680
[(4AAP)(PA)]	281	4.426	1.06×10^4	1.98×10^4	17.07	31.93	11.21	32.70	1.25	−34,357

Determination of ionization potential (I_P) of the donor

The ionization potentials (I_P) of the 4AAP donor in the complexes were calculated using the empirical equation derived by Aloisi and Pignataro represented in the following equation [36]:

$$I_P(eV) = 5.76 + 1.53 \times 10^{-4} v_{CT} \quad (5)$$

where v_{CT} is the wavenumber in cm^{-1} that corresponds to the CT band formed from the interaction between the donor and the acceptor. The electron-donating power of a donor molecule is measured by its ionization potential, which is the energy required to remove an electron from the highest occupied molecular orbital.

Determination of resonance energy (R_N)

Briegleb and Czekalla [37] theoretically derived the following relationship to obtain the resonance energy (R_N):

$$\varepsilon_{CT} = 7.7 \times 10^{-4} / [h v_{CT} / [R_N] - 3.5] \quad (6)$$

where ε_{CT} is the molar absorptivity coefficient of the CT complex at the maximum of the CT absorption, v_{CT} is the frequency of the CT peak, and R_N is the resonance energy of the complex in the ground state, which contributes to the stability constant of the complex (a ground-state property).

Determination of energy of the charge-transfer complex (E_{CT})

The energy values (E_{CT}) of the $n \rightarrow \pi^*$ and π–π^* interactions between the donor (4AAP) and the acceptors were calculated using the equation derived by Briegleb [38]:

$$E_{CT} = (h v_{CT}) = (1243.667 / \lambda_{CT}) \quad (7)$$

where λ_{CT} is the wavelength of the CT band.

Determination of standard free energy changes (ΔG^o)

The standard free energy of complexation (ΔG^o) for each complex was calculated from the formation constants using the equation derived by Martin et al. [39]:

$$\Delta G^\circ = -2.303 RT \log K_{CT} \quad (8)$$

where ΔG^o is the free energy of the CT complexes (kJ mol^{-1}), R is the gas constant (8.314 J mol^{-1} K^{-1}), T is the absolute temperature in K, and K_{CT} is the formation constant of the complex (L mol^{-1}) at room temperature.

The calculated spectroscopic and physical values (f, μ, I_P, R_N and ΔG^o) for the 4AAP complexes using these equations are presented in Table 2. [(4AAP)(QL)] exhibits higher values for both the oscillator strength (f) and the transition dipole moment (μ). These high f values indicate a strong interaction between the donor–acceptor pairs with relatively high probabilities of CT transitions [40]. One important aspect of characterizing CT complexes is the calculation of the ionization potential (I_P) of the donor. The calculated I_P value for the highest filled molecular orbital that participates in the CT interaction of the 4AAP is approximately 11.15. The ionization potential of the electron donor has been reported to be correlated with the charge-transfer transition energy of the complex [41]. Further evidence for the nature of the CT interactions is the calculation of the standard free energy change (ΔG^o). The obtained values of ΔG^o for the 4AAP/QL and 4AAP/PA complexes are −38 and −34 kJ mol^{-1}, respectively; these values indicate that the interaction between 4AAP and the acceptors is exothermic and spontaneous. In general, ΔG^o values are more negative as the formation constants of the CT complexes increase.

IR and Raman spectra

The assignments for the characteristic IR and Raman spectral bands for the complexes are shown in Table 3, whereas the full assignment of the IR bands in the spectrum is listed in Tables 4 and 5. The full IR and Raman spectra of the CT complexes are shown in Figs. 4 and 5, respectively. The formation of the CT complexes during the reaction of 4AAP with QL or PA is strongly supported by the observation of main infrared bands of the donor (4AAP) and acceptors (QL and PA) in the product spectra. However, the bands of the donor and acceptors in the spectra of the complexes reveal small changes in frequency and in their band intensities compared with those of the free donor and acceptors. This result could be attributed to the expected changes in symmetry and electronic structure upon the formation of the CT complexes. The characteristic bands of 4AAP observed at 3432 and 3326 cm^{-1}, which are assigned to -NH_2 asymmetric and symmetric stretching vibrations, respectively [42], shifted to lower values and reduced in intensity after complexation. This observation clearly indicates that the —NH_2 group in the donor participates in the complexation process. The IR spectra of the 4AAP/QL and 4AAP/

Table 3
Assignments of the characteristic IR and Raman spectral bands (cm^{-1}) for [(4AAP)(QL)] and [(4AAP)(PA)] complexes.

Complex	ν(NH)		$\delta(NH_3^+)_{def}$		$\delta(NH_3^+)_{sym}$		$\rho\Delta(NH_3^+)$	
	IR	Raman	IR	Raman	IR	Raman	IR	Raman
[(4AAP)(QL)]	3213	3064	1588	1595	1314	1327	832	854
[(4AAP)(PA)]	3345	3082	1564	1580	1318	1313	837	826

Table 4
Characteristic infrared frequencies (cm^{-1})[a] and tentative assignments for 4AAP, QL and their complex.

4AAP	QL	Complex [(4AAP)(QL)]	Assignments [b]
			ν(N—H); 4AAP
3432 ms		3737 w	ν_{as}(C—H); 4AAP
3326 ms	3262 br	3390 w	ν(O—H); QL
3207 s	3031 m	3316 mw	ν(C—H); aromatic
		3213 br	$\nu(NH_3^+)$
	2857 m		
–	2836 m	2840 w	ν_s(C—H)+ν_{as}(C—H)
	2716 m	2731 m, br	Hydrogen bonding
–		2593 w	
	2590 w	2471 vw	Over tone/ combination
	2467 vw	2361 m	
1651 vs	–	1608 vs	ν(C=O); 4AAP
			(N—H) scissoring; 4AAP
	1628 w		$\delta(NH_3^+)_{def}$, complex
1590 ms	1609 w	1588 vs	ν(C=C) (in-ring), aromatic
	1518 vs	1507 vs	ν(C=O)+ν(C=N)
			δ(C—H) deformation
			Ring breathing bands
1498 ms			ν(C—H); alkanes; 4AAP
1456 s	1477 vs	1466 sh, s	ν(C=C) (in-ring), aromatic
			δ(C—H) deformation
			$\delta(NH_3^+)_{sym}$, complex
1353 ms	1366 ms	1363 m	ν(C—C)+ν(C—O)+ν_{as}(C—N)
		1314 s	C—H rock, alkanes; 4AAP
1311 m			
1274 ms	1244 vs	1242 s	ν_s(C—N); 4AAP
1230 m	1222 vs	1215 sh, s	ν(C—O); 4AAP, QL
1118 m	1210 vs	1139 vw	δ(C—H) in plane bending
1074 m	1164 ms	1096 w	δ_{rock}; NH
	1097 m		
1025 m			
			$\rho(NH_3^+)$, complex
			C—H out of plane bending
759 vs	827 s	832 ms	δ_{rock}, CH_2 rock
	759 vs	764 vs	N—H wagging
			Skeletal vibrations
			N—H twisting
572 m	616 m	698 ms	N—CH_3 wagging
501 m	525 ms	579 m	CNC deformation
		521 mw	

[a] s, strong; w, weak; m, medium; sh, shoulder; v, very; vs very strong; br, broad.
[b] ν, stretching; ν_s , symmetrical stretching; ν_{as} , asymmetrical stretching; δ, bending.

Table 5
Characteristic infrared frequencies (cm^{-1})[a] and tentative assignments for 4AAP, PA and their complex.

4AAP	PA	Complex [(4AAP)(PA)]	Assignments [b]
			ν(N—H); 4AAP
3432 ms	3416 br	3427 m, br	ν_{as}(C—H); 4AAP
3326 ms	3103 ms	3345 m	ν(O—H); PA
3207 s			ν(C—H); aromatic
			$\nu(NH_3^+)$
–	2980 sh	2926 m, br	ν_s(C—H)+ν_{as}(C—H)
	2872 w		Hydrogen bonding
–	–	2362 mw	Over tone/ combination
1651 vs	–	1633 vs	ν(C=O); 4AAP
			(N—H) scissoring; 4AAP
	1632 vs		$\nu_{as}(NO_2)$; PA
1590 ms	1608 vs	1564 s	$\delta(NH_3^+)_{def}$, complex
	1529 vs	1492 s	ν(C=C) (in-ring), aromatic
			ν(C=O)+ν(C=N)
			δ(C—H) deformation
			Ring breathing bands
1498 ms			ν(C—H); alkanes; 4AAP
1456 s	1432 s	1435 m	ν(C=C) (in-ring), aromatic
			δ(C—H) deformation
			$\delta(NH_3^+)_{sym}$, complex
1353 ms	1343 ms	1364 m	ν(C—C)+ν(C—O)+ν_{as}(C—N)
	1312 w	1318 vs	C—H rock, alkanes; 4AAP
			$\nu_s NO_2$
1311 m		1271 m	
1274 ms	1263 w	1162 m	ν_s(C—N); 4AAP
1230 m	1150 ms	1126 w	ν(C—O); 4AAP
1118 m	1086 s	1078 m	δ(C—H) in plane bending
1074 m	917 vs	913 m	δ_{rock}; NH
1025 m			
	829 w	837 mw	($\rho(NH_3^+)$), complex
759 vs	781 s	766 mw	C—H out of plane bending
	732 s	714 s	δ_{rock}, CH_2 rock
			N—H wag
			skeletal vibrations
572 m	703 s	703 ms	N—H twisting
501 m	652 sh	666 mw	N—CH_3 wagging
	522 ms	575 m	δ(ONO); PA
			CNC deformation

[a] s, strong; w, weak; m, medium; sh, shoulder; v, very; vs very strong; br, broad.
[b] ν, stretching; ν_s , symmetrical stretching; ν_{as} , asymmetrical stretching; δ, bending.

PA complexes are characterized by a broad medium band that appears between 2400–2800 cm^{-1} (2731 cm^{-1} for the QL complex; 2926 cm^{-1} for the PA complex), which does not appear in the spectra of the free 4AAP donor or those of the QL and PA acceptors. These broadened peaks are due to hydrogen bonding in the complex formed through the transfer of a proton from QL or PA to the amine of 4AAP [43]. This assumption is strongly supported by the appearance of the characteristic absorption bands that result from the stretching and bending deformation of the NH_3^+ group. IR and Raman spectra confirm the presence of these bands; the *v(NH)*, $\nu_{def}(NH_3^+)$, $\delta_{sym}(NH_3^+)$ and $\rho(NH_3^+)$ absorptions are observed for [(4AAP)(QL)] and [(4AAP)(PA)] at approximately 3200, 1600, 1300 and 800 cm^{-1}, respectively. The presence of these bands confirmed that the complexation occurs through the protonation of the 4AAP amine by the phenolic groups of the acceptors [44–48].

^{1}H NMR spectra

The 400 MHz ^{1}H NMR spectra of the complexes were measured in DMSO-d_6 at room temperature and are given in Fig. 6. The chemical shifts (δ) of the different types of protons of the CT complexes are given below. The results obtained from the elemental analyses, infrared spectra, and photometric titrations are in agreement with the ^{1}H NMR spectra, which allows for an interpretation of the mode of interaction between the donor and the acceptor. The reaction of 4AAP with QL yielded a new charge-transfer complex, 1,5-dimethyl-3-oxo-2-phenyl-2,3-dihydro-1*H*-pyrazol-4-aminium-4-

hydroxyphenolate, which produced signals (Fig. 6) at Δ = 2.09 (s, 3H, CH_3, antipyrine C3), 2.73 (s, 3H, N-CH_3), 3.83 (s, 3H, $-NH_3^+$), 6.56 (s, 4H, Ar—H, quinol ring protons), 7.21 (t, 1H, Ar—H, phenyl C4), 7.34 (m, 2H, Ar—H, phenyl C3 and C5), 7.50 (t, 2H, Ar—H, phenyl C2 and C6), 8.59 (s, 1H, Ar—OH, 4-hydroxyphenolate). The ^{1}H NMR spectrum of this complex displays two signals of equal intensity at 2.09 ppm (3H) and 2.73 ppm (3H), corresponding to the protons of C—CH_3 and N—CH_3 groups, respectively [49,50]. The spectrum indicated that the phenolic proton (—OH) signal, which is observed at approximately 9 ppm in the spectrum of the QL acceptor, decreased in intensity with an upfield shift (8.59 ppm). This result indicates the involvement of the phenolic group in the chelation of the donor via deprotonation and an overall decrease in the negative charge on the quinol ring due to the formation of the complex. In addition, the disappearance of the —NH_2 protons from 4AAP and the appearance of a weak broad band at 3.83 ppm, which is attributed to the ammonium protons, indicate the involvement of the amine group in the complexation process. Based on these data, the structure suggested for the 4AAP/QL complex is shown in Formula II.

The ^{1}H NMR spectrum for the CT complex formed with 4AAP and PA is shown in Fig. 6 and is summarized as follows: Δ = 2.27 (s, 3H, CH_3, antipyrine C3), 3.02 (s, 3H, N—CH_3), 3.89 (s, 3H, $-NH_3^+$), 7.34 (t, 1H, Ar—H, phenyl C4), 7.36 (m, 2H, Ar—H, phenyl C3 and C5), 7.50 (t, 2H, Ar—H, phenyl C2 and C6), 8.59 (s, 2H, Ar—H, picrate C3 and C5). In the charge-transfer reaction between 4AAP and PA, the proton of the —OH group of PA is transferred to the amine of 4AAP to form an ion-paired compound named 1,5-dimethyl-3-oxo-2-phenyl-2,3-dihydro-1*H*-pyrazol-4-aminium-2,4,6-trinitrophenolate. The two signals of equal intensity at 2.27 ppm (3H) and 3.02 ppm (3H), corresponding to the protons of C—CH_3 and N—CH_3 groups, respectively [49,50]. The new peak observed at 3.89 ppm in the complex, which is not detected in the spectrum of the free donor, is attributed to the formation of a hydrogen bond [51] between PA and 4AAP. The peak at δ = 11.94 ppm, which is assigned to the —OH proton of picric acid [52], was absent in the spectrum of this complex. Together, these data indicate that the amine and phenolic groups are involved in the formation of the CT complex between 4AAP and PA. The intensities and chemical shifts of the aromatic signals were significantly affected by the complexation process and the accompanying changes in the structural configuration. According to these observations, the suggested structure for the 4AAP/PA complex is illustrated in Formula III.

Thermal analysis

To examine the thermal stability of the new complexes, the thermogravimetric analysis of the complexes were carried out over the temperature range of 25–800 °C under an air atmosphere. The TG curves were redrawn as mass loss versus temperature. Typical TG curves of the complexes are presented in Fig. 7, and the

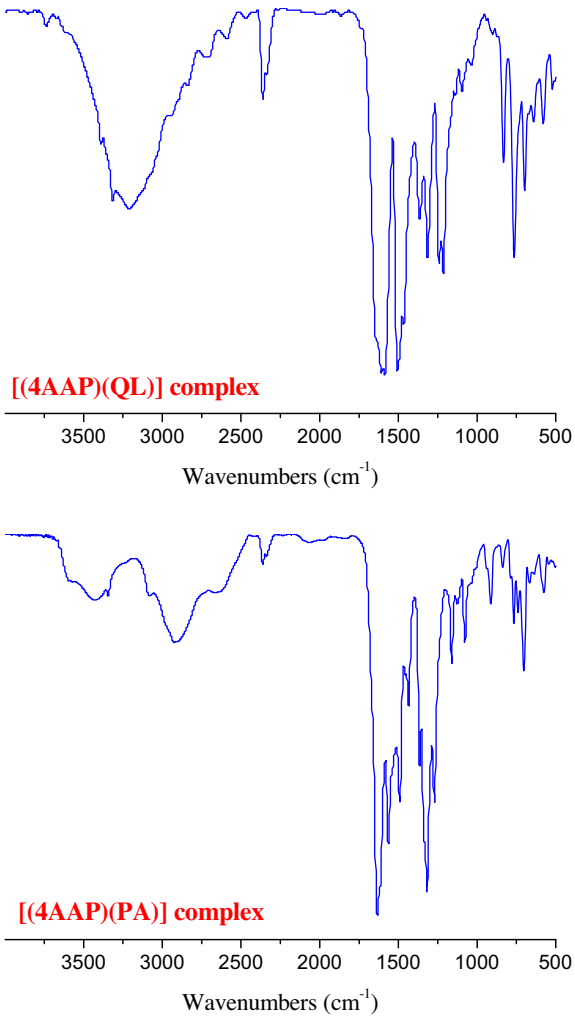

Fig. 4. Infrared spectra of 4AAP CT complexes.

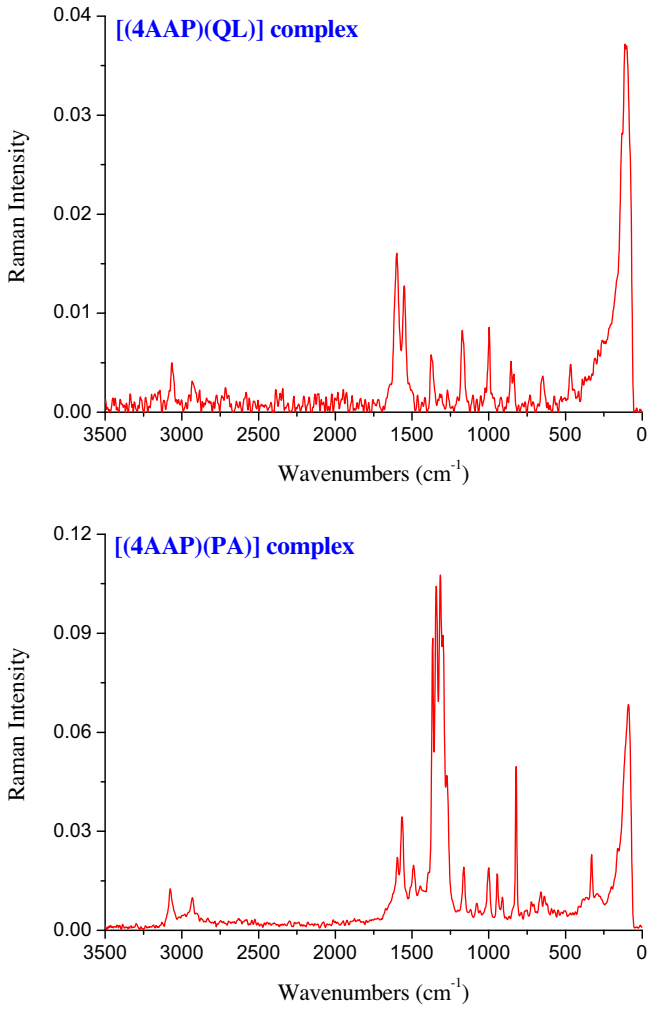

Fig. 5. Raman spectra of 4AAP CT complexes.

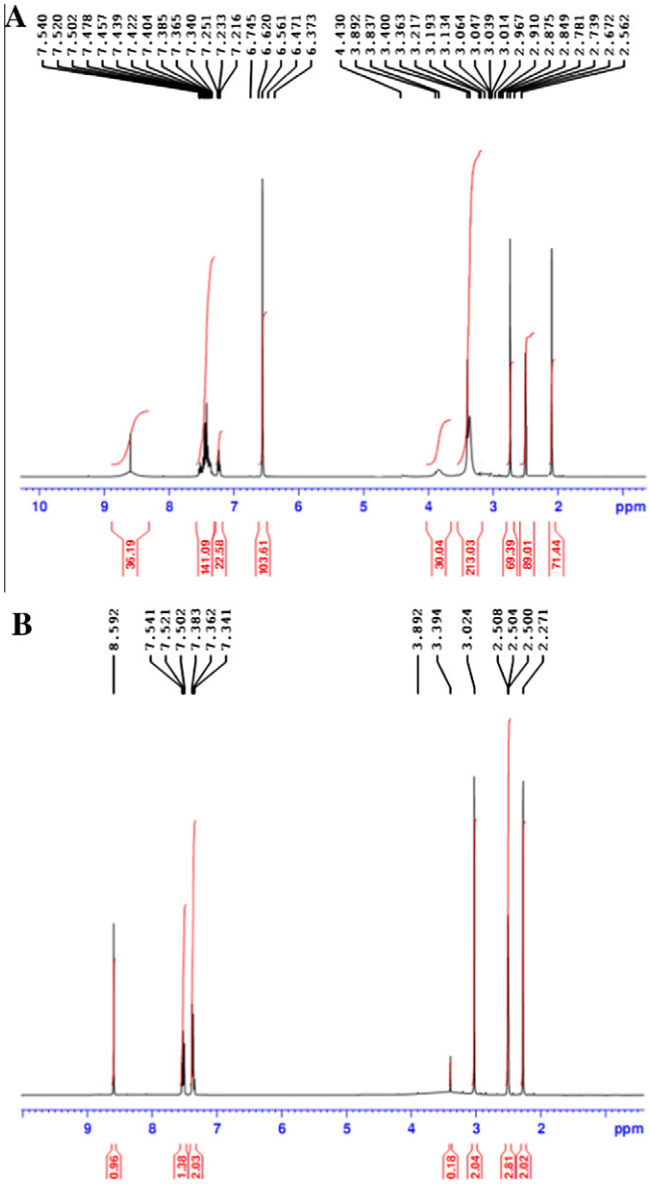

Fig. 6. ^{1}H NMR spectrum of (A) 4AAP-QL and (B) 4AAP-PA complexes.

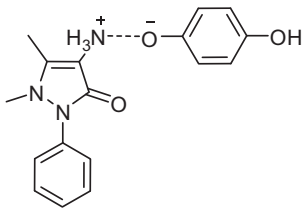

Formula II. Suggested structure of the [(4AAP)(QL)] complex.

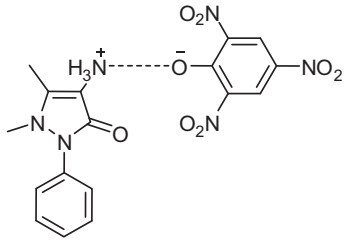

Formula III. Suggested structure for the [(4AAP)(PA)] complex.

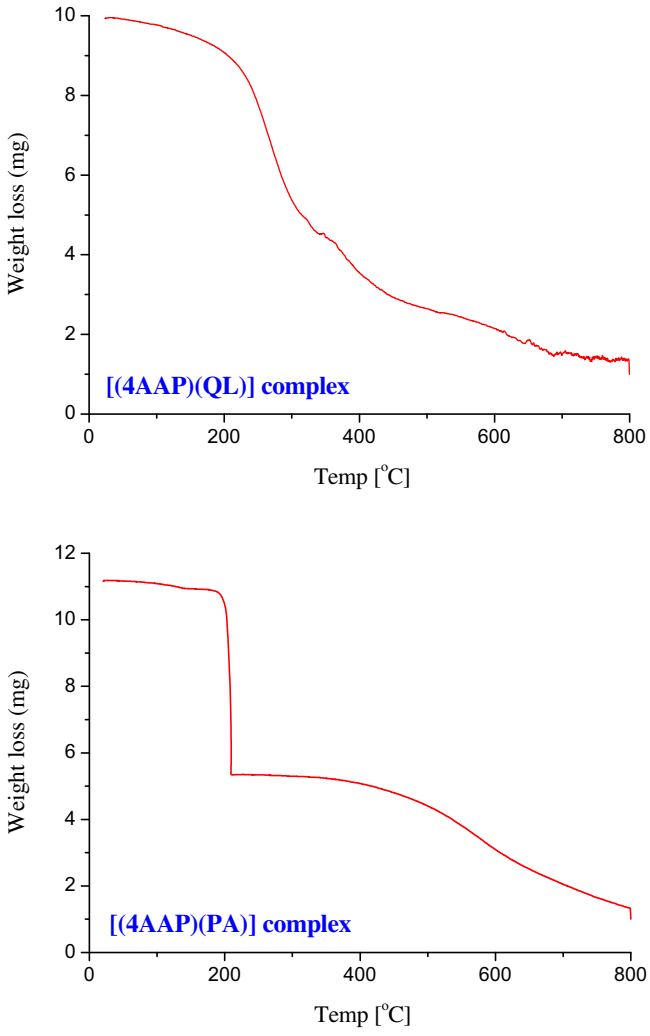

Fig. 7. TG curves of 4AAP CT complexes.

thermoanalytical results are listed in Table 6. Comparison of the thermograms revealed that [(4AAP)(PA)] is more stable than [(4AAP)(QL)].

The thermal analysis curve of [(4AAP)(QL)] indicates that its decomposition begins at ~80 °C and finishes at ~640 °C. The decomposition reactions of the complex occur in two main stages within the given temperature range. The first stage of decomposition within the temperature range of 25–320 °C proceeds with a weight loss value of 48.55%. This stage might be associated with loss of 3 C_2H_2, CO_2, NH_3 and NO_2 molecules in good agreement with the calculated value of 48.83%. The second stage of decomposition proceeds within the temperature range of 320–800 °C and corresponds to the liberation of 3 C_2H_2, NO_2 and 2 H_2 molecules. The weight loss associated with this stage (35.75%) is in excellent agreement with the calculated value (35.74%). The total mass loss is 84.3% with only carbon remaining as a final residue. [(4AAP)(PA)] begins to decompose at ~180 °C in two clear decomposition steps within the 25–800 °C temperature range. The first decomposition step within the temperature range of 25–220 °C (obs. = 52.10%, calc. = 53.43%) is attributed to the liberation of 2 C_2H_2, 2 CO_2, NH_3 and 3 NO_2 molecules. The second decomposition

Table 6
Thermal decomposition data for the 4AAP CT complexes.

Complex	Stage	TG range (°C)	Mass loss (%)		Evolved moiety
			Found	Calculated	
[(4AAP)(QL)] ($C_{17}H_{19}N_3O_3$)	I	25–320	48.55	48.83	$3C_2H_2+CO_2+NH_3+NO_2$
	II	320–800	35.75	35.74	$3C_2H_2+NO_2+2H_2$
	Residue	–	15.70	15.32	Residual carbons
[4AAP)(PA)] ($C_{17}H_{16}N_6O_8$)	I	25–220	52.10	53.43	$2C_2H_2+2CO_2+NH_3+3NO_2$
	II	220–800	35.99	35.39	$3C_2H_2+CO_2+NH_3+NO_2$
	Residue	–	11.91	11.10	Residual carbons

Table 7
Kinetic parameters determined using the Coats–Redfern (CR) and Horowitz–Metzger (HM).

Complexes	Stage	Method	Parameters[a]					r
			E^*	A	ΔS^*	ΔH^*	ΔG^*	
[(4AAP)(QL)]	1st	CR	7.46×10^4	7.04×10^4	-1.57×10^2	7.02×10^4	1.54×10^5	0.99289
		HM	7.97×10^4	5.82×10^5	-1.39×10^2	7.53×10^4	1.49×10^5	0.98919
[(4AAP)(PA)]	1st	CR	6.19×10^5	1.25×10^6	1.02×10^3	6.15×10^5	1.27×10^5	0.95530
		HM	6.14×10^5	4.53×10^6	1.01×10^2	6.10×10^5	1.26×10^5	0.95055

[a] Units of parameters: E in kJ mol^{-1}, A in s^{-1}, ΔS in J mol^{-1}K^{-1}, ΔH and ΔG in kJ mol^{-1}.

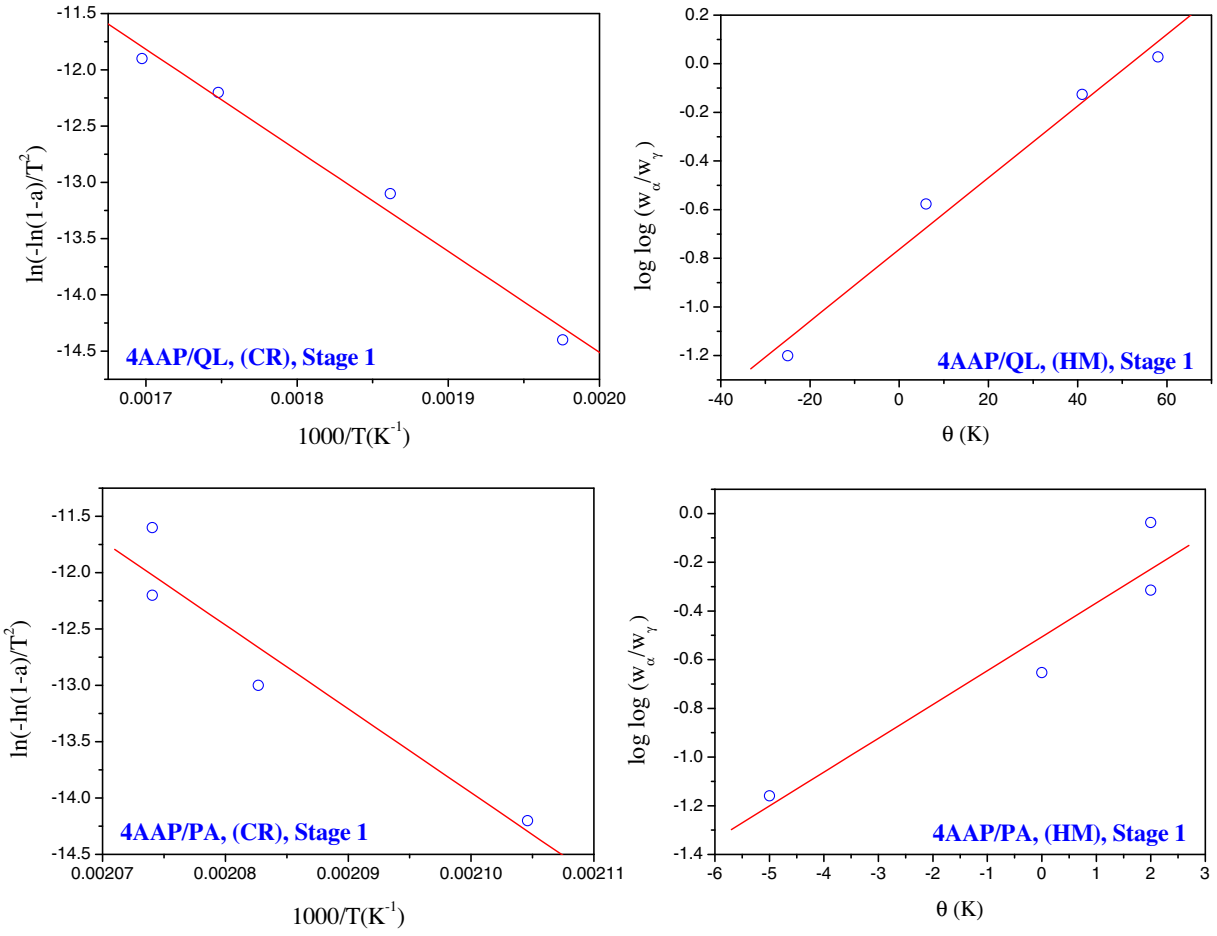

Fig. 8. The diagrams of kinetic parameters of 4AAP complexes using Coats–Redfern (CR) and Horowitz–Metzger (HM) equations.

step within the 220–800 °C temperature range (obs. = 35.99%, calc. = 35.39%) is reasonably explained by the loss of 3 C_2H_2, CO_2, NH_3 and NO_2 molecules. The overall loss of mass by this complex is 88.1%.

Kinetic and thermodynamic studies

Kinetic studies on thermal processes are expected to provide information regarding the Arrhenius parameters, such as the

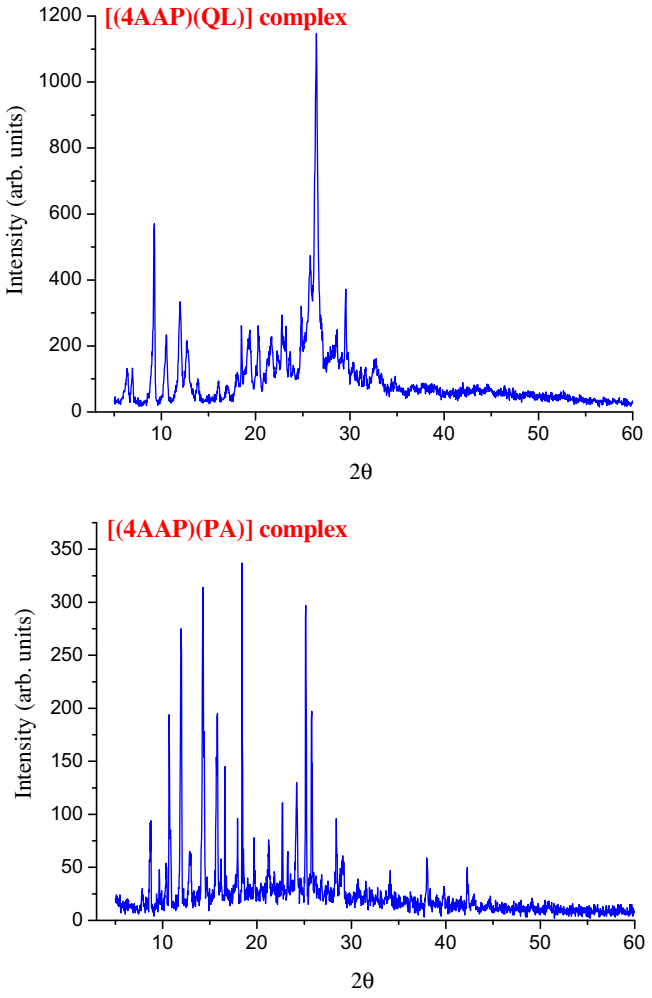

Fig. 9. X-ray diffraction pattern for [(4AAP)(QL)] and [(4AAP)(PA)] complexes.

Table 8
XRD spectral data of 4AAP CT complexes.

Complex	2θ (°)	d value (Å)	Full width at half maximum (FWHM)	Relative intensity (%)	Particle size (nm)
[(4AAP)(QL)]	26.278	3.386	0.35	100	4.25
[(4AAP)(PA)]	18.480	4.800	0.15	100	9.78

activation energy (E^*), the frequency factor (A), the enthalpy of activation (H^*), the entropy of activation (S^*), and the free energy of activation (G^*). Two methods were used to evaluate the kinetic thermodynamic parameters: the Coats–Redfern method [53] and the Horowitz–Metzger [54] method.

Coats–Redfern equation

The Coats–Redfern Eq. (9), which is an atypical integral method, can be represented as:

$$\int_{0\to\infty} d\alpha/(1-\alpha)^n = (A/\varphi)\int_{T1\to T2} e^{-E^*/RT}dT \tag{9}$$

For convenience, the lower limit T_1 is usually taken as zero. After integration, this equation can be represented as:

$$\mathrm{Ln}[-\ln(1-\alpha)/T^2] = -E^*/RT + \ln[AR/\varphi E^*] \tag{10}$$

where α is the fraction of the sample decomposed at time t, T is the derivative peak temperature, A is the frequency factor, R is the gas constant, E^* is the activation energy, and φ is the linear heating rate. A plot of the left-hand side (LHS) against $1/T$ was constructed. E^* is the activation energy in kJ mol^{-1} and was calculated from the slope. The A (s^{-1}) value was calculated from the intercept. The entropy of activation, ΔS^*, in (J K^{-1} mol^{-1}) was calculated using the equation:

$$\Delta S^* = R\ln(Ah/kT_s) \tag{11}$$

where k is the Boltzmann constant, h is Planck's constant, and T_s is the DTG peak temperature.

Horowitz–Metzger equation

The Horowitz–Metzger equation (Eq. (12)) is given in the following form:

$$\log[\log(w_\alpha/w_\gamma)] = E^*\theta/2.303RT_s^2 - \log 2.303 \tag{12}$$

where $\theta = T - T_s$, $w_\gamma = w_\alpha - w$, w_α is the mass loss at the completion of the reaction, and w is the mass loss at time t.

The plot of log [log (w_α/w_γ)] versus θ was constructed and was observed to be linear, and E^* was calculated from its slope. The pre-exponential factor, A, was calculated from the following equation:

$$E^*\theta/RT_s^2 = A/[\varphi\exp(-E^*/RT_s)] \tag{13}$$

From the TG curves, the activation energy, E^*, the entropy of activation, ΔS^*, the enthalpy of activation, ΔH^*, and the Gibbs free energy, ΔG^*, were calculated from:

$$\Delta H^* = E^* - RT \quad \text{and} \quad \Delta G^* = \Delta H^* - T\Delta S^*$$

The evaluated kinetic parameters for the first stages based on the Coats–Redfern and Horowitz–Metzger equations are listed in Table 7, and the linear curves from the Coats–Redfern and Horowitz–Metzger plots are shown in Fig. 8. The results indicate that the kinetic data obtained from the two methods are comparable and in agreement with each other. The activation energy of the complexes is expected to increase with increasing thermal stability of complexes. Hence, the E^* value for [(4AAP)(PA)] is much higher than for [(4AAP)(QL)], which indicates the higher thermal stability of [(4AAP)(PA)]. The calculated E^* values using the Coats–Redfern and Horowitz–Metzger methods for the main decomposition stage of the complexes are found to be 6.17×10^5 kJ mol^{-1} for [(4AAP)(PA)] and 7.72×10^4 kJ mol^{-1} for [(4AAP)(QL)]. Satisfactory values for the correlation coefficients from the Arrhenius plots of the thermal decomposition steps were observed to be r ~1 in all cases, which indicates a good fit with the linear function and reasonable agreement between the experimental data and the kinetic parameters. The negative values of ΔS^* observed for [(4AAP)(QL)] indicate that the reaction rate is slower than normal [55].

X-ray powder diffraction investigation

To investigate the crystal structures of the complexes, X-ray powder diffraction patterns in the range of $5 < 2\theta < 60°$ for the obtained complexes were examined, and the recorded patterns are shown in Fig. 9. The main characteristic scattering peak of [(4AAP)(QL)] occurs at 26.278°, whereas this peak occurs at 18.480° for [(4AAP)(PA)]. Based on these investigations, the sharp and well-defined Bragg peaks at specific 2θ angles confirm the semi-crystalline nature of the investigated CT complexes. The particle size of these two complexes were estimated from their XRD patterns based on the highest intensity value compared with the other peaks using the well-known Debye–Scherrer formula given in the Eq. (14) [56]:

$$D = K\lambda/\beta\cos\theta \tag{14}$$

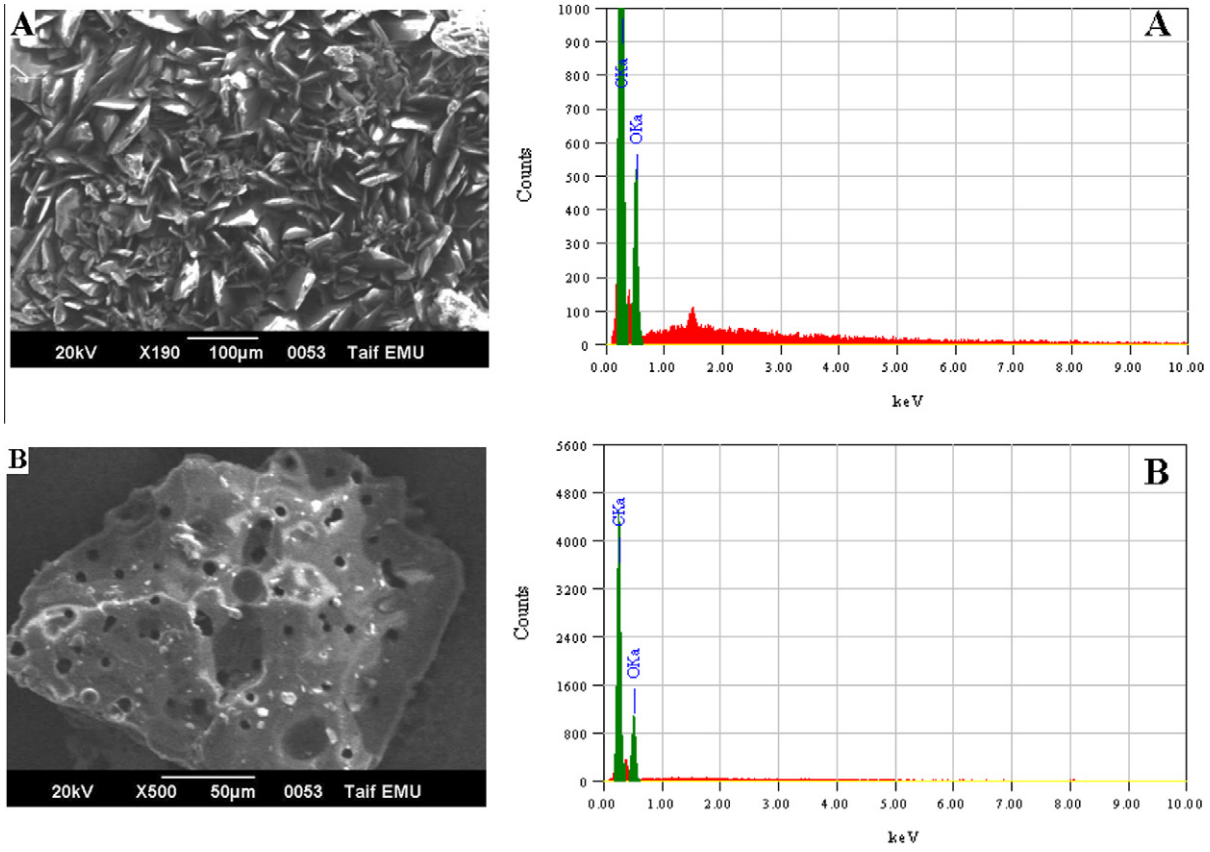

Fig. 10. SEM images and EDX spectra of (A) [(4AAP)(QL)] and (B) [(4AAP)(PA)] complexes.

Table 9
The inhibition diameter zone values (mm) for 4AAP and its CT complexes.

Sample		Inhibition zone diameter (mm/mg sample)					
		Bacteria			Fungi		
		Bacillus subtilis, (G^+)[a]	*Escherichia coli*, (G^-)	*Pseudomonas aeuroginosa*, (G^-)	*Staphylococcus aureus*, (G^+)	*Aspergillus flavus*	*Candida albicans*
Control: DMSO		0.0	0.0	0.0	0.0	0.0	0.0
Standard	Tetracycline (antibacterial agent)	34.0	32.0	34.0	30.0	–	–
	Amphotericin B (antifungal agent)	–	–	–	–	18.0	19.0
4AAP		6	7	5	6	0.0	0.0
[(4AAP)(QL)]		20.0	20.0	17.0	22.0	12.0	17.0
[(4AAP)(PA)]		11.0	13.0	12.0	12.0	0.0	0.0

[a] G: Gram reaction.

where D is the apparent particle size of the grains, K is a constant (0.94 for Cu grid), λ is the X-ray wavelength used (1.5406 Å), θ is half the scattering angle (the Bragg diffraction angle), and β is the full-width at half-maximum (FWHM) of the X-ray diffraction line (additional peak broadening) in radians. Table 8 presents the XRD spectral data for the complexes. The particle sizes of the complexes were estimated according to the highest intensity value compared with the other peaks and were found to be ~4 and ~10 nm for the [(4AAP)(QL)] and [(4AAP)(PA)] complexes, respectively. These values confirmed that the particle sizes are within the nanoscale range.

SEM and EDX studies

The morphological features of the complexes were investigated using scanning electron microscopy (SEM). SEM provides general information about the microstructure, surface morphology, particle size, chemical composition and porous structures of the surfaces. Fig. 10 shows the SEM surface images of the complexes along with their EDX spectra. The analysis of the SEM images of the complexes showed the following:

- The morphological phases of these complexes have a homogeneous matrix, as indicated by the uniformity and similarity of the particles of the synthesized CT complexes.
- The sizes of the particles are quite different with different acceptors.
- The complexes are semi-crystalline, and some single-phase formations exhibit well-defined shapes.
- The [(4AAP)(QL)] particles exhibit different flake shapes containing sharp edges with a particle size of ~100 µm.
- The [(4AAP)(PA)] particles are sponge-shaped with a porous nature and a particle size of ~50 µm.

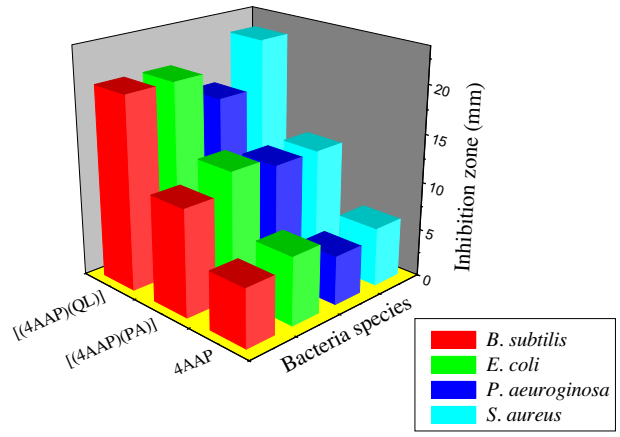

Fig. 11. Statistical representation for antibacterial activity of 4AAP and its complexes.

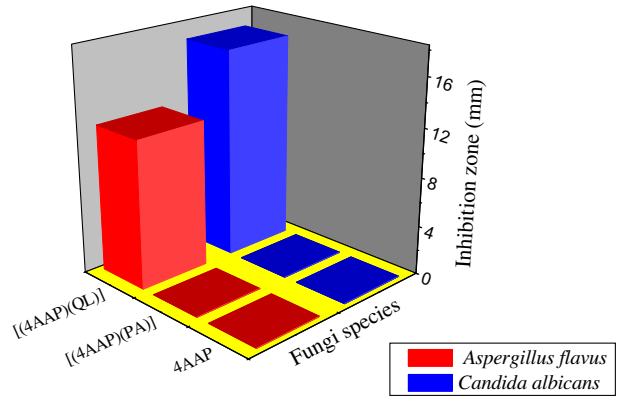

Fig. 12. Statistical representation for antifungal activity of 4AAP and its complexes.

In addition, the chemical compositions of the complexes were determined using energy-dispersive X-ray diffraction (EDX). The chemical analysis results from the EDX analysis for the formed complexes showed a homogeneous distribution of each acceptor. In the EDX profile, the peaks refer to all elements that constitute the molecules of these complexes; these elements were clearly identified, and the results confirmed the proposed structures.

Pharmacology

The 4AAP and its CT complexes were screened in vitro for their antibacterial and antifungal activity. The CT complexes to be tested were dissolved in DMSO to obtain 100 μg/ml stock solutions. The diameter zones were measured to determine their effects on the growth of the tested microorganisms.

Antibacterial activity studies

The antibacterial activity of the 4AAP and its complexes were tested in vitro against two Gram-positive bacterial strains, *S. aureus* (*S. aureus*) and *B. subtilis*, and two Gram-negative bacterial strains, *E. coli* (*E. coli*) and *P. aeruginosa* (*P. aeruginosa*). The activity was determined by measuring the inhibition zone diameter values (mm) of the complexes against the microorganisms. Tetracycline was used as a positive control. The screening data are given in Table 9 and are statistically presented in Fig. 11. The data reveal that the [(4AAP)(QL)] complex showed good inhibitory activity against the growth of the tested bacterial strains. The [(4AAP)(PA)] complex exhibited moderate inhibitory results against all of the Gram-positive and Gram-negative bacterial species, as reported in Table 9.

Antifungal activity studies

The 4AAP and its synthesized CT complexes were also screened for their antifungal properties against two fungal species, *A. flavus* and *C. albicans*. Amphotericin B was used as a positive control, and the screening data are reported in Table 9 and statistically presented in Fig. 12. The data revealed that the [(4AAP)(QL)] complex had a significant antifungal response against *C. albicans*. The [(4AAP)(PA)] complex exhibited no inhibitory activity against either fungal species, as shown in Table 9. It is obvious that the antimicrobial activities of the 4AAP CT complexes are more than that of free 4AAP. The [(4AAP)(QL)] complex shows good antifungal activities, while the free 4AAP has no such activity which makes this complex of interest. The most reasons for lethal action of tested 4AAP CT complexes may be due to their interactions with critical intracellular sites causing the death of cells. The variety of antimicrobial activities of tested 4AAP CT complexes may due to a different degree of tested complexes penetration through cell membrane structure of target organism [57].

Conclusion

Structural studies of the newly synthesized charge-transfer complexes of 4-aminoantipyrine (4AAP) with quinol (QL) and picric acid (PA) were carried out. Two new proton-transfer salts, named 1,5-dimethyl-3-oxo-2-phenyl-2,3-dihydro-1*H*-pyrazol-4-aminium-4-hydroxyphenolate and 1,5-dimethyl-3-oxo-2-phenyl-2,3-dihydro-1*H*-pyrazol-4-aminium-2,4,6-trinitrophenolate for QL and PA, respectively, are formed via a 1:1 donor/acceptor stoichiometry. The IR, Raman and ^{1}H NMR spectra show that the complexes formed between 4AAP and QL or PA are stabilized by hydrogen bonding, which is formed between the phenolic group of the acceptors and the primary amine of 4AAP. The obtained complexes are nanoscale, semi-crystalline particles, and the compound formed with PA is thermally stable up to 180 °C with a remarkable sponge-like morphology. The antibacterial and antifungal activities of the newly synthesized CT complexes were studied using the disc diffusion method, and [(4AAP)(QL)] exhibited good microbial activities against various bacterial and fungal strains compared with standard drugs.

References

[1] Y.M. Chen, Y.P. Chen, Fluid Phase Equilibr. 282 (2009) 82.
[2] Y. Teng, F. Ji, C. Li, Z. Yu, R. Liu, J. Lumin. 131 (2011) 2661.
[3] Y. Teng, R. Liu, C. Li, H. Zhang, J. Hazard. Mater. 192 (2011) 1766.
[4] A. Lang, C. Hatscher, C. Wiegert, P. Kuhl, Amino Acids 36 (2009) 333.
[5] V. Mishra, R. Kumar, Carbohydr. Polym. 86 (2011) 296.
[6] A. Lang, C. Hatscher, P. Kuhl, Tetra. Lett. 48 (2007) 3371.
[7] S. Cunha, S.M. Oliveira, M.T. Rodriques, R.M. Bastos, J. Ferrari, C.M.A. de Oliveira, L. Kato, H.B. Napolitano, I. Vencato, C. Lariucci, J. Mol. Struct. 752 (2005) 32.
[8] S. Prasad, R.K. Agarwal, Transit. Metal Chem. 32 (2007) 143.
[9] J.F. Van Staden, N.W. Beyene, R.I. Stefan, H.Y. Aboul-Enein, Talanta 68 (2005) 401.
[10] J. Kasthuri, J. Santhanalakshmi, N. Rajendiran, Transit. Metal Chem. 33 (2008) 899.
[11] C.Z. Katsaounos, E.K. Paleologos, D.L. Giokas, M.I. Karayannis, Int. J. Environ. Anal. Chem. 83 (2003) 507–514.
[12] A.M. Farghaly, A. Hozza, Pharmazie 35 (1980) 596.
[13] D. Chiaramonte, J.M. Steiner, J.D. Broussard, K. Baer, S. Gumminger, E.M. Moller, D.A. Williams, R. Shumway, Can. J. Vet. Res. 67 (2003) 183.
[14] P.M. Selvakumar, E. Suresh, P.S. Subramanian, Polyhedron 26 (2007) 749.
[15] N.L. Olenovich, L.I. Koval Chuk, Zh. Anal. Khim 28 (1975) 2162.
[16] Y. Teng, R. Liu, C. Li, Q. Xia, P. Zhang, J. Hazard. Mater. 190 (2011) 574.
[17] A.M. Vinagre, E.F. Collares, Braz. J. Med. Biol. Res. 40 (2007) 903.
[18] S.G. Sunderji, A. El Badry, E.R. Poore, J.P. Figueroa, P.W. Nathanielsz, Am. J. Obstet. Gynecol. 149 (1984) 408.

[19] S.C. Pierre, R. Schmidt, C. Brenneis, M. Michaelis, G. Geisslinger, K. Scholich, Brit. J. Pharmacol. 151 (2007) 494.
[20] Y. Teng, R. Liu, S. Yan, X. Pan, P. Zhang, M. Wang, J. Fluoresc. 20 (2010) 381.
[21] S. Chandra, D. Jain, A.K. Sharma, P. Sharma, Molecules 14 (2009) 174.
[22] N. Raman, S. Sobha, A. Thamaraichelvan, Spectrochim. Acta A78 (2011) 888.
[23] N. Raman, S. Sobha, Inorg. Chem. Commun. 17 (2012) 120.
[24] M.R. Saber, F.A. Mauther, J. Mol. Struct. 1020 (2012) 177.
[25] D.A. Skoog, Principle of Instrumental Analysis, third ed., Saunders, New York, USA, 1985 (Chapter 7).
[26] H.A. Benesi, J.H. Hildebrand, J. Am. Chem. Soc. 71 (1949) 2703.
[27] R. Abu-Eittah, F. Al-Sugeir, Can. J. Chem. 54 (1976) 3705.
[28] A.W. Bauer, W.M. Kirby, C. Sherris, M. Turck, Am. J. Clin. Pathol. 45 (1966) 493.
[29] M.A. Pfaller, L. Burmeister, M.A. Bartlett, M.G. Rinaldi, J. Clin. Microbiol. 26 (1988) 1437.
[30] D.J. Beecher, A.C. Wong, Appl. Environ. Microbiol. 60 (1994) 1646.
[31] National Committee for Clinical Laboratory Standards. Methods for Antimicrobial Susceptibility Testing of Anaerobic Bacteria: Approved Standard M11-A3. NCCLS, Wayne, PA, USA, 1993.
[32] National Committee for Clinical Laboratory Standards. Reference Method for Broth Dilution Antifungal Susceptibility Testing of Conidium-Forming Filamentous Fungi: Proposed Standard M38-A. NCCLS, Wayne, PA, USA, 2002.
[33] National Committee for Clinical Laboratory Standards. Method for Antifungal Disk Diffusion Susceptibility Testing of Yeast: Proposed Guideline M44-P. NCCLS, Wayne, PA, USA, 2003.
[34] H. Tsubomura, R.P. Lang, J. Am. Chem. Soc. 83 (1961) 2085.
[35] R. Rathone, S.V. Lindeman, J.K. Kochi, J. Am. Chem. Soc. 119 (1997).
[36] G. Aloisi, S. Pignataro, J. Chem. Soc. Faraday Trans. 69 (1972) 534.
[37] G. Briegleb, J. Czekalla, Z. Physikchem. Frankfurt 24 (1960) 237.
[38] G. Briegleb, Z. Angew. Chem. 72 (1960) 401 (Z. Angew. Chem. 76 (1964) 326).
[39] A.N. Martin, J. Swarbrick, A. Cammarata, Physical Pharmacy, third ed., Lee and Febiger, Philadelphia, PA, 1969. p. 344.
[40] M.S. Refat, A. Elfalaky, E. Elesh, J. Mol. Struct. 990 (2011) 217.
[41] M. Pandeeswaran, K.P. Elango, Spectrochim. Acta A 65 (2006) 1148.
[42] J. Swaminathan, M. Ramalingam, V. Sethuraman, N. Sundaraganesan, S. Sebastian, Spectrochim. Acta A 73 (2009) 593.
[43] M.S. Refat, L.A. El-Zayat, O.Z. Yesilel, Spectrochim. Acta A 75 (2010) 745.
[44] M.S. Refat, H.A. Saad, A.A. Adam, J. Mol. Struct. 995 (2011) 116.
[45] L.J. Bellamy, The Infrared Spectra of Complex Molecules, Chapman & Hall, London, 1975.
[46] R. Bharathikannan, A. Chandramohan, M.A. Kandhaswamy, J. Chandrasekaran, R. Renganathan, V. Kandavelu, Cryst. Res. Technol. 43 (6) (2008) 683.
[47] A.S. Gaballa, S.M. Teleb, E. Nour, J. Mol. Struct. 1024 (2012) 32.
[48] A.A. Adam, J. Mol. Struct (2012).
[49] R.M. Issa, A.M. Kheder, H.F. Rizk, Spectrochim. Acta A 62 (2005) 621.
[50] S. Fazil, R. Ravindran, A.S. Devi, B.K. Bijili, J. Mol. Struct. 1021 (2012) 147.
[51] N. Singh, A. Ahmad, J. Mol. Struct. 977 (2010) 197.
[52] R.D. Kross, V.A. Fassel, J. Am. Chem. Soc. 79 (1957) 38.
[53] A.W. Coats, J.P. Redfern, Nature (London) 201 (1964) 68.
[54] H.H. Horowitz, G. Metzger, Anal. Chem. 35 (1963) 1464.
[55] A.A. Frost, R.G. Pearson, Kinetics and Mechanism, Wiely, New York, NY, USA, 1961.
[56] S.J.S. Qazi, A.R. Rennie, J.K. Cockcroft, M. Vickers, J. Colloid Interface Sci. 338 (2009) 105.
[57] A.A. El-Habeeb, F.A. Al-Saif, M.S. Refat, J. Mol. Struct. 1034 (2013) 1.